Quantum Transport in Si:P δ-Layer Wires

Juan P. Mendez
Cognitive & Emerging Computing
Sandia National Laboratories
Albuquerque, USA
jpmende@sandia.gov

Denis Mamaluy
Cognitive & Emerging Computing
Sandia National Laboratories
Albuquerque, USA
dnmamal@sandia.gov

Xujiao Gao
Electrical Models & Simulation
Sandia National Laboratories
Albuquerque, USA
xngao@sandia.gov

Evan M. Anderson
Multiscale Fab. Sci. & Tech. Dev.
Sandia National Laboratories
Albuquerque, USA
emander@sandia.gov

DeAnna M. Campbell
Biological & Chemical Sensors
Sandia National Laboratories
Albuquerque, USA
dmlope@sandia.gov

Jeffrey A. Ivie
Multiscale Fab. Sci. & Tech. Dev.
Sandia National Laboratories
Albuquerque, USA
jaivie@sandia.gov

Tzu-Ming Lu
Quantum Phenomena
Sandia National Laboratories
Albuquerque, USA
tlu@sandia.gov

Scott W. Schmucker
Multiscale Fab. Sci. & Tech. Dev.
Sandia National Laboratories
Albuquerque, USA
swschmu@sandia.gov

Shashank Misra
Multiscale Fab. Sci. & Tech. Dev.
Sandia National Laboratories
Albuquerque, USA
smisra@sandia.gov

***Abstract*—We employ a fully charge self-consistent quantum transport formalism, together with a heuristic elastic scattering model, to study the local density of state (LDOS) and the conductive properties of Si:P δ-layer wires at the cryogenic temperature of 4 K. The simulations allow us to explain the origin of shallow conducting sub-bands, recently observed in high resolution angle-resolved photoemission spectroscopy experiments. Our LDOS analysis shows the free electrons are spatially separated in layers with different average kinetic energies, which, along with elastic scattering, must be accounted for to reproduce the sheet resistance values obtained over a wide range of the δ-layer donor densities.**

***Index Terms*—quantum transport, Si:P δ-layer systems, contact block reduction, NEGF, elastic scattering**

I. Introduction

The electronic structure and conductive properties of Si:P δ-layer systems have been a subject of experimental [1]–[5] and computational [6], [7] works due to the high potential for beyond-Moore computational applications. However, many discrepancies persist among these studies, and many questions still remain open, such as how many conductive modes exist, or the influence of the δ-layer thickness and doping density on these conductive modes. Previous studies were based on traditional closed-system quantum approaches, either tight-binding [6] or DFT [7]. However, these approaches rely on two essential approximations: 1) the closed-system approximation that attempts to represent the density of states of a highly conductive system as $DOS(E) = \sum_\alpha \delta(E - E_\alpha)$ and thus neglecting the quantum wire (continuum) states; 2) the (semi)classical approximations for the extraction of systems' conductive properties assuming that the current is proportional to the electron density $j \sim n$ instead of the quantum-mechanical flux $j \sim \Psi\nabla\Psi^* - \Psi^*\nabla\Psi$ (that is zero for any closed system wave-function Ψ). In this work, we have employed a fully charge self-consistent open-system quantum transport (QT) formalism [8]–[10], which is free of the above mentioned approximations, together with an elastic scattering model, to study the conduction sub-band structure and the corresponding conductive properties of Si:P δ-layer systems.

This work is funded under Laboratory Directed Research and Development Grand Challenge (LDRD GC) program, Project No. 213017, at Sandia National Laboratories. Sandia National Laboratories is a multimission laboratory managed and operated by National Technology and Engineering Solutions of Sandia, LLC., a wholly owned subsidiary of Honeywell International, Inc., for the U.S. Department of Energy's National Nuclear Security Administration under contract DE-NA-0003525. This paper describes objective technical results and analysis. Any subjective views or opinions that might be expressed in the paper do not necessarily represent the views of the U.S. Department of Energy or the United States Government.

II. Methodology and model

A. Quantum transport method

To conduct this study, we have employed a quantum-mechanical transport framework for open systems [8]–[10] that relies on a fully charge self-consistent solution of the Poisson-open system Schrödinger equation in the single-band (Γ-valley) effective mass approximation. Fig. 1 shows a detailed flow chart of the method implemented in the QT simulator. For a numerically efficient implementation of the Non-Equilibrium Green's Function (NEGF) formalism we utilized the Contact Block Reduction (CBR) method [8], [9]; for the charge self-consistent solution of the non-linear Poisson equation we employed a combination of the open-system predictor-corrector approach and Anderson mixing scheme [10], [11]. The standard values of electron effective masses $m_l = 0.98 \times m_e$, $m_t = 0.19 \times m_e$ and the dielectric constant

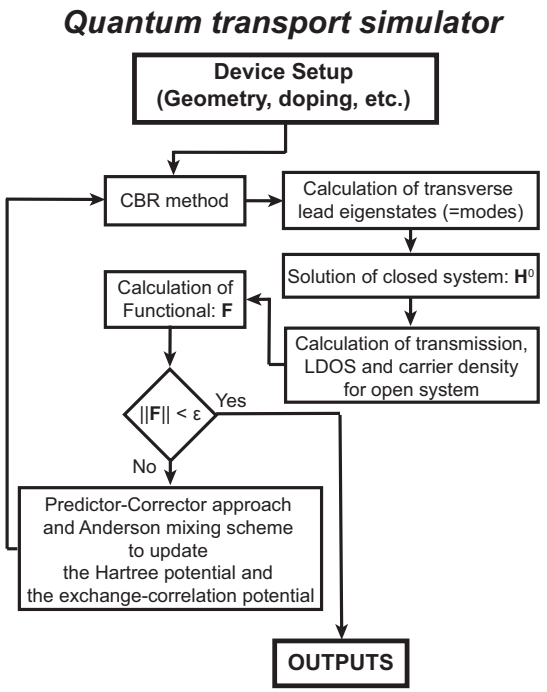

Fig. 1. Flow chart of the self-consistent QT method. ϵ is the Poisson residuum tolerance.

$\epsilon_{Si} = 11.7$ of Silicon were employed in our calculations, as well as the cryogenic temperature of 4 K.

B. Elastic scattering model

We can distinguish two types of elastic scattering that can occur in a device: 1) geometry scattering, due to the ohmic contacts, doping profile, device geometry, etc.; and 2) defect scattering, due to defects, vacancies, impurities, etc. [12], [13]. The former one is already taken into account by the charge self-consistent QT framework. However, the second one needs explicitly to be included in this framework. Thus, we introduce a heuristic elastic defect scattering model for meso- and macroscopic scale, which treats the defects as abstract scatterers. We consider that scatterers are spatially equally distributed along the conductor channel and can be defined by a linear defect density ν. Fig. 2 shows the schematic elastic scattering model, formed by M modes with N_m scatterers, where $m = 1, ..., M$. In general, each transmission mode can possess a different linear defect density $\nu_m = N_m/L$, where L is the length of the channel device. If the electronic transmission for mode m across the conductor without scatterers is giving by $T_{mm}(E)$ at energy E, then the effective electronic transmission for mode m including N_m scatterers can be computed as [14]

$$\frac{1 - T^{\text{eff}}_{mm}(E)}{T^{\text{eff}}_{mm}(E)} = \frac{1 - T_{mm}(E)}{T_{mm}(E)} + \sum_{i=1}^{N} \frac{1 - t'^{(i)}_{mm}(E)}{t'^{(i)}_{mm}(E)}, \qquad (1)$$

where $t'^{(i)}_{mm}(E)$ is the defect transmission probability due to scatterer i in mode m. The first term in (1) accounts for geometry scattering, whereas the second term encompasses

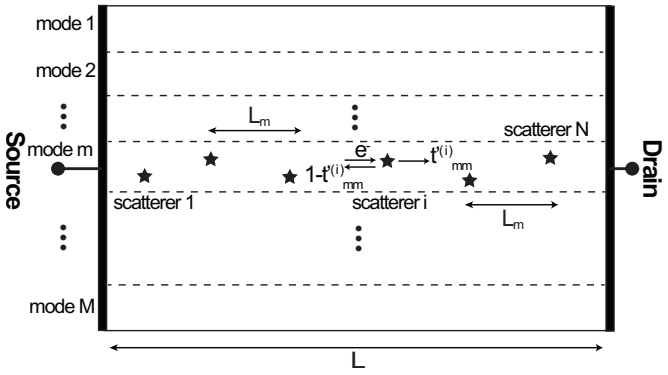

Fig. 2. Schematic elastic scattering model.

for defect scattering. In absence of defects, i.e. $t'^{(i)}_{mm}(E) = 1$ with $i = 1, ..., N$, the effective transmission function $T^{eff}_{mm}(E)$ reduces to $T_{mm}(E)$, as expected. If we assume that the defect transmission probability is the same for all scatterers, i.e. $t'^{(i)}_{mm}(E) = t'_{mm}(E)$, the effective transmission probability can be rewritten as

$$T^{\text{eff}}_{mm}(E) = \frac{1}{1 + \frac{1-T_{mm}(E)}{T_{mm}(E)} + L\nu_m \frac{1-t'_{mm}(E)}{t'_{mm}(E)}}. \qquad (2)$$

The term $\nu_m(1 - t'_{mm})/t'_{mm}$ is of the order of 1/L_m [14], where L_m is the mean free path. Therefore, it can be approximated as α/L_m, where α is an adjustable parameter that is proportional to the linear defect density in the system. More complex elastic scattering models can be employed in this framework, e.g., models in which the defect transmission probability is energy-dependent.

The total current density J from source to drain can be then calculated from the Landauer formula as

$$J = \frac{2e}{h} \int \sum_{m=1}^{M} T^{eff}_{mm}(E)\big(f_S(E) - f_D(E)\big)dE, \qquad (3)$$

where e is the electron charge and h is the Planck's constant. The equilibrium distribution functions for source and drain leads are $f_S(E)$ and $f_D(E)$, respectively.

C. Computational model

The geometry of the Si: P δ-layer wire is shown in Fig. 3, which is composed of a Si body, a very high P-doped layer, and a Si cap. The conductor channel is in contact with two semi-infinite leads, the source and drain, respectively. For simplicity, we only focus on symmetric configurations, where the widths, W, and acceptor doping concentrations, N_A, of the body and cap are chosen to be the same. Asymmetric doping would result in an asymmetric electron distribution around the δ-layer plane. Similarly, we chose the body and cap widths as large as possible to avoid additional border effects on the electron confinement around the δ-layer ($W = 10$ nm). The wire length is set to $L = 50$ nm. An acceptor doping density in the Si body/cap of 1.0×10^{17} cm^{-3} was used throughout this work.

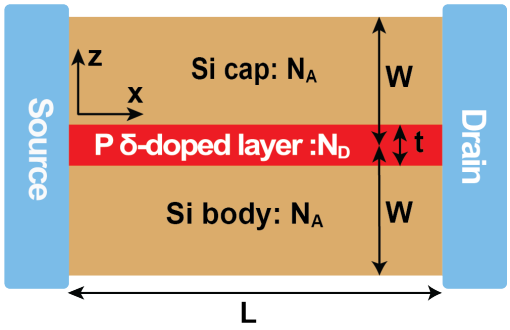

Fig. 3. Schematic model for Si: P δ-layer wires.

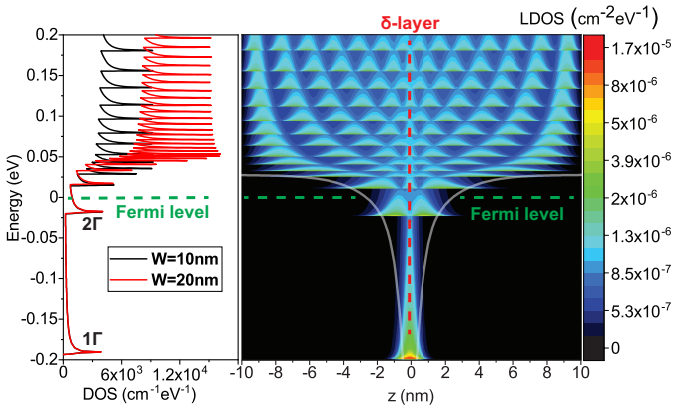

Fig. 4. Left panel: DOS for Si:P δ-layer wires with different widths, W = 20 nm and 40 nm. Right panel: LDOS(z,E) for a 20 nm-width Si:P δ-layer wire. For both panels, t = 0.2 nm, $N_D = 1.2 \times 10^{14}$ cm^{-2} and $N_A = 1.0 \times 10^{17}$ cm^{-3}.

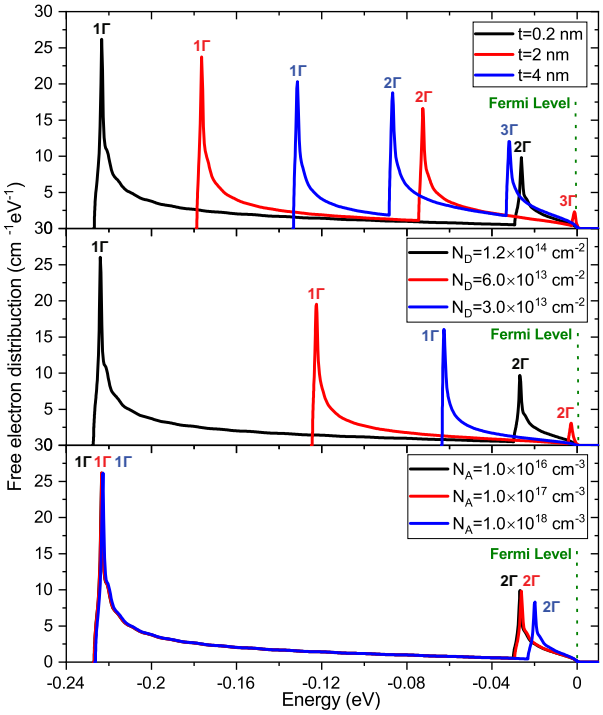

Fig. 5. Upper panel: influence of δ-layer thickness t on the free electron distribution for a fixed sheet doping density of $N_D = 1.2 \times 10^{14}$ cm^{-2} ($N_A = 1.0 \times 10^{17}$ cm^{-3}). Middle panel: influence of sheet doping density N_D on the free electron distribution for a fixed 0.2 nm δ-layer thickness ($N_A = 1.0 \times 10^{17}$ cm^{-3}). Lower panel: influence of the Si cap/body doping N_A on the free electron distribution for a fixed 0.2 nm δ-layer thickness and a donor doping of $N_D = 1.2 \times 10^{14}$ cm^{-2}.

III. Results and Discussion

A. Electronic structure

The DOS of the system at equilibrium conditions is included in the left panel of Fig. 4. The DOS results reveal the presence of conducting sub-bands (below the Fermi level) corresponding to 1Γ and 2Γ valleys, respectively, recently observed in high-resolution angle-resolved photoemission spectroscopy experiments (ARPES) [4], [5]. To get a better insight of the electronic structure in Si: P δ-layer systems, we take a look at the LDOS(E,z) in the YZ plane, included in the right panel of Fig. 4 for a 20 nm-width wire. The LDOS presents a peculiar quantization of the modes in space and energy, which we have referred to as "Quantum Menorah". The occupied modes below the Fermi level are independent of the encapsulation depth of δ-layer from the surfaces of the Si cap/body, as shown in the left panel of Fig. 4 for $W = 20$ and 40 nm. The LDOS also reveals that the free electrons are strongly confined spatially around the δ-layer, however, they are distributed in layers with different kinetic energies.

Our simulations also indicate that the number of sub-bands and the corresponding structure is strongly influenced by the thickness and doping density of the δ-layer, as shown in Fig. 5 (upper and middle panel). The effect of the Si body/cap doping on the conduction sub-bands turns out to be secondary, as shown in the lower panel of Fig. 5. For a fixed δ-layer thickness, the increment of the sheet doping increases the number of conducting modes, as well as the splitting energy between them. In contrast, for a fixed sheet doping, the increment of the δ-layer thickness increases the number of modes, but decreases the energy splitting between them, which is in agreement with the ARPES observation in [5]. This is the result of the electronic confinement around the δ-layer: smaller layer thickness and higher doping create a stronger potential well (see right panel of Fig. 4) that leads to higher electronic confinement around the δ-layer and, therefore, an increased energy difference between sub-bands.

B. Conductive properties

With our QT framework and the elastic scattering model for meso- and macroscopic scale, we can compute the sheet conductance of the system. The results are included in Fig. 6 for a wide range of donor doping concentration, from 4.0×10^{11} cm^{-2} to 5.0×10^{14} cm^{-2}, and δ-layer thicknesses, from 2 nm to 5 nm. To account for the linear increase of the mean free path L_m with the sheet doping density reported in [15], we approximated the term $\nu_m(1 - t'_{mm})/(t'_{mm})$ in (2) as $\alpha/L_m(N_D)$, where the values of $L_m(N_D)$ were taken from [15] and α was set to 1.0. Moreover, our simulations reproduce the experimental sheet resistance data (see Fig. 7) obtained by several groups [15]–[18]. From our conductive

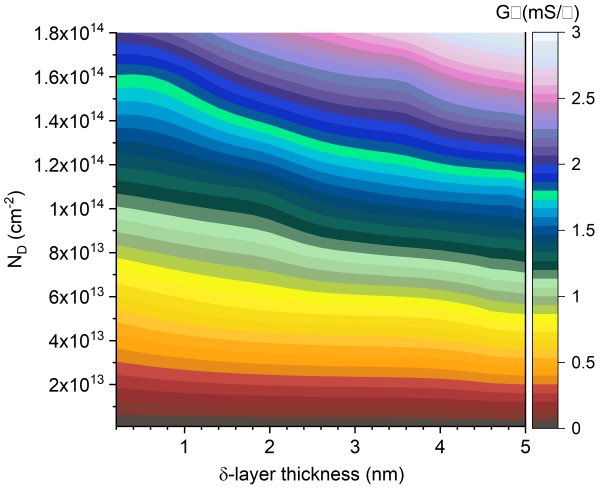

Fig. 6. Sheet conductance for Si:P δ-layer wires in function of the δ-layer thickness and doping density (for the linear impurity density $\alpha = 1.0$)

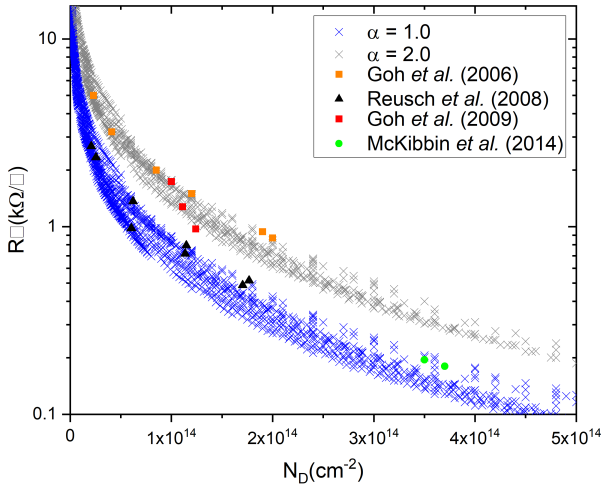

Fig. 7. Comparison of the sheet resistance for different δ-layer thicknesses, from 2 nm to 8 nm, and doping densities against experimental data [15]–[18].

results, we can distinguish two regimes, corresponding to high P doping densities (above 5.0×10^{13} cm^{-2}) and low doping density (below 1.0×10^{13} cm^{-2}), which present dissimilar behavior. The conductance of the system raises with the δ-layer thickness for a fixed sheet doping density. However, our simulations indicate that the slope of the conductance vs thickness becomes steeper as we move to higher doping densities. In the limits, the conductance is strongly dependent on the δ-layer thickness for high doping densities, whereas it remains approximately invariant for low doping densities.

IV. Conclusion

Our simulations allow us to explain the origin of shallow conducting sub-bands, recently observed in ARPES experiments. The LDOS analysis reveals a peculiar structure that we have termed as "quantum menorah", as well as the free electrons are spatially separated by layers with different average kinetic energies. The number of conductive sub-bands is mainly determined by the thickness and sheet doping density of the δ-layer. The effect of the acceptor doping density in the Si body/cap is secondary and negligible. Furthermore, by applying an elastic scattering model in our QT framework, we reproduce the sheet resistance values measured by various experimental groups. Finally, we report that the conductance of the system increases with the increment of the δ-layer thickness for high sheet doping densities.

References

[1] D. Ward, S. Schmucker, E. Anderson, E. Bussmann, L. Tracy, T.-M. Lu, L. Maurer, A. Baczewski, D. Campbell, M. Marshall, and S. Misra, "Atomic precision advanced manufacturing for digital electronics," *Electronic Device Failure Analysis*, vol. 22, no. 1, pp. 4–10, 2020.

[2] Y. He, S.K.Gorman, and D. Keith et al., "A two-qubit gate between phosphorus donor electrons in silicon," *Nature*, vol. 571, pp. 371–375, 2019.

[3] J. Wyrick, X. Wang, R. V. Kashid, P. Namboodiri, S. W. Schmucker, J. A. Hagmann, K. Liu, M. D. Stewart Jr., C. A. Richter, G. W. Bryant, and R. M. Silver, "Atom-by-atom fabrication of single and few dopant quantum devices," *Adv. Funct. Mater.*, vol. 29, no. 52, p. 1903475, 2019.

[4] F. Mazzola, C.-Y. Chen, R. Rahman, X.-G. Zhu, C. M. Polley, T. Balasubramanian, P. D. King, P. Hofmann, J. A. Miwa, and J. W. Wells, "The sub-band structure of atomically sharp dopant profiles in silicon," *npj Quantum Mater.*, vol. 5, no. 34, 2020.

[5] A. J. Holt, S. K. Mahatha, R.-M. Stan, F. S. Strand, T. Nyborg, D. Curcio, A. K. Schenk, S. P. Cooil, M. Bianchi, J. W. Wells, P. Hofmann, and J. A. Miwa, "Observation and origin of the Δ manifold in Si:P δ layers," *Phys. Rev. B*, vol. 101, p. 121402, 2020.

[6] S. Lee, H. Ryu, H. Campbell, L. C. L. Hollenberg, M. Y. Simmons, and G. Klimeck, "Electronic structure of realistically extended atomistically resolved disordered Si:P δ-doped layers," *Phys. Rev. B*, vol. 84, p. 205309, 2011.

[7] D. J. Carter, O. Warschkow, N. A. Marks, and D. R. McKenzie, "Electronic structure models of phosphorus δ-doped silicon," *Phys. Rev. B*, vol. 79, p. 033204, 2009.

[8] D. Mamaluy, M. Sabathil, and P. Vogl, "Efficient method for the calculation of ballistic quantum transport," *J. Appl. Phys.*, vol. 93, no. 8, pp. 4628–4633, 2003.

[9] D. Mamaluy, D. Vasileska, M. Sabathil, T. Zibold, and P. Vogl, "Contact block reduction method for ballistic transport and carrier densities of open nanostructures," *Phys. Rev. B*, vol. 71, p. 245321, 2005.

[10] X. Gao, D. Mamaluy, E. Nielsen, R. W. Young, A. Shirkhorshidian, M. P. Lilly, N. C. Bishop, M. S. Carroll, and R. P. Muller, "Efficient self-consistent quantum transport simulator for quantum devices," *J. Appl. Phys.*, vol. 115, no. 13, p. 133707, 2014.

[11] H. R. Khan, D. Mamaluy, and D. Vasileska, "Quantum transport simulation of experimentally fabricated nano-finfet," *IEEE T. Electron Dev.*, vol. 54, no. 4, pp. 784–796, 2007.

[12] J. Mendez, F. Arca, J. Ramos, M. Ortiz, and M. Ariza, "Charge carrier transport across grain boundaries in graphene," *Acta Mater.*, vol. 154, pp. 199 – 206, 2018.

[13] F. Arca, J. P. Mendez, M. Ortiz, and M. P. Ariza, "Charge-carrier transmission across twins in graphene," *J. Phys. Condens. Matter*, vol. 32, no. 42, p. 425003, 2020.

[14] S. Datta, *Electronic transport in mesoscopic systems*. Cambridge university press, 1997.

[15] K. E. J. Goh, L. Oberbeck, M. Y. Simmons, A. R. Hamilton, and M. J. Butcher, "Influence of doping density on electronic transport in degenerate Si:P δ-doped layers," *Phys. Rev. B*, vol. 73, p. 035401, 2006.

[16] K. E. J. Goh and M. Y. Simmons, "Impact of si growth rate on coherent electron transport in Si:P delta-doped devices," *Appl. Phys. Lett.*, vol. 95, no. 14, p. 142104, 2009.

[17] S. R. McKibbin, C. M. Polley, G. Scappucci, J. G. Keizer, and M. Y. Simmons, "Low resistivity, super-saturation phosphorus-in-silicon monolayer doping," *Appl. Phys. Lett.*, vol. 104, no. 12, p. 123502, 2014.

[18] T. C. G. Reusch, K. E. J. Goh, W. Pok, W.-C. N. Lo, S. R. McKibbin, and M. Y. Simmons, "Morphology and electrical conduction of Si:P δ-doped layers on vicinal si(001)," *J. Appl. Phys.*, vol. 104, no. 6, p. 066104, 2008.